

## Effects of different joint wall lengths on in-plane compression properties of 3D braided jute/epoxy composite honeycombs

Qian-Qian, Li; Mosleh, Yasmine; Alderliesten, R.C.; Hong-Hua, Zhang; Wei, Li

**DOI**

[10.1177/07316844231167898](https://doi.org/10.1177/07316844231167898)

**Publication date**

2023

**Document Version**

Final published version

**Published in**

Journal of Reinforced Plastics & Composites

**Citation (APA)**

Qian-Qian, L., Mosleh, Y., Alderliesten, R. C., Hong-Hua, Z., & Wei, L. (2023). Effects of different joint wall lengths on in-plane compression properties of 3D braided jute/epoxy composite honeycombs. *Journal of Reinforced Plastics & Composites*, 43(9-10), 547-564. <https://doi.org/10.1177/07316844231167898>

**Important note**

To cite this publication, please use the final published version (if applicable).  
Please check the document version above.

**Copyright**

Other than for strictly personal use, it is not permitted to download, forward or distribute the text or part of it, without the consent of the author(s) and/or copyright holder(s), unless the work is under an open content license such as Creative Commons.

**Takedown policy**

Please contact us and provide details if you believe this document breaches copyrights.  
We will remove access to the work immediately and investigate your claim.

***Green Open Access added to TU Delft Institutional Repository***


***'You share, we take care!' - Taverne project***

**<https://www.openaccess.nl/en/you-share-we-take-care>**

Otherwise as indicated in the copyright section: the publisher is the copyright holder of this work and the author uses the Dutch legislation to make this work public.

# Effects of different joint wall lengths on in-plane compression properties of 3D braided jute/epoxy composite honeycombs

Li Qian-Qian<sup>1,2</sup> , Yasmine Mosleh<sup>3</sup> , RC Alderliesten<sup>4</sup>, Zhang Hong-Hua<sup>1,2</sup> and Li Wei<sup>1,2,5</sup> 

*Journal of Reinforced Plastics and Composites*  
2023, Vol. 0(0) 1–18  
© The Author(s) 2023  
Article reuse guidelines:  
[sagepub.com/journals-permissions](https://sagepub.com/journals-permissions)  
DOI: 10.1177/07316844231167898  
[journals.sagepub.com/home/jrp](https://journals.sagepub.com/home/jrp)  


## Abstract

To comply with the trend in the development of engineering materials towards lightweight, high strength, eco-friendly, sustainable, and multi-functional, a three-dimensional braided integrated composite honeycomb is designed. The effects of geometrical parameters particularly joint wall lengths on the in-plane mechanical behavior of the honeycombs were investigated. The results show that the in-plane mechanical properties are related to the number of cell walls, and the angle between the cell wall and the loading direction. Increasing the number of cell rows to double and triple at similar areal density lead to an improvement of the maximum load up to 2.5, and 3.8 times, respectively. Similarly, the total absorbed strain energy increased up to 2.6 and 5.9 times, respectively. The displacement at the maximum load is increased by 1.6 and 2.7 times as a result of increasing the cell row number. The total absorbed strain energy increased to 1.7 and 1.3 times, respectively. The failure angle of the 3D braided composite honeycomb is about 4°–7°. This investigation presents the geometrical factors of a 3D braided composite honeycomb can be further designed and optimized, but it also provides a reference for the development and design of a new composite honeycomb.

## Keywords

3D braiding, in-plane compression, composite honeycombs, jute, failure analysis

## Introduction

As a cellular structure, the honeycomb structure has been attracting more and more attention for its immaculate regularity and excellent mechanical behavior at low relative densities.<sup>1–3</sup> The honeycomb is considered a stable and effectively optimized structure consisting of uniformly distributed hexagonal cells. The material selection is a pivotal design parameter when developing new honeycomb structures. In comparison to aluminum and Nomex honeycombs, fiber-reinforced composites exhibit higher specific stiffness and strength which shows the potential for developing advanced lightweight structures with enhanced mechanical properties.<sup>3</sup> There is an increasing interest in lignocellulosic plant fibers as reinforcement in polymer matrix composites.<sup>4</sup>

In addition to the material, the manufacturing technique is also a crucial factor to enable a wider range of applications for fiber-reinforced polymer honeycombs (FRPH). Stocchi<sup>5</sup> introduced two methods of manufacturing jute fabric reinforced vinylester matrix honeycomb structure, one is using a mold with fixed inserts and another is using a mold that can be compressed laterally. The tailor-folding method is proposed by Wei<sup>6</sup> to make an all-composite sandwich panel with a carbon fiber-reinforced polymer (CFRP) hexagon honeycomb core.

Pehlivan and Baykasoğlu<sup>7</sup> put forward the corrugation technique, in which the prepreg CFRP sheets were first corrugated into a certain shape using corrugated aluminum molds under heat and pressure, and then the corrugated CFRP sheets were glued and stacked to construct honeycomb specimens. The simpler and more convenient preparation method is the tailor-foldin<sup>6,8</sup> method or the interlockin<sup>9</sup> method. However, the integrity of honeycombs produced with these methods is rather poor. In a high-temperature and high-humidity environment or when subjected to alternating forces, the bonding area is prone

<sup>1</sup>Shanghai Collaborative Innovation Center for High Performance Fiber Composites, Donghua University, Shanghai, China

<sup>2</sup>Donghua University, College of Textiles, Shanghai, China

<sup>3</sup>Bio-Based Structures and Materials, Faculty of Civil Engineering and Geosciences, TU Delft, Delft, Netherlands

<sup>4</sup>Structural Integrity and Composites, Faculty of Aerospace Engineering, TU Delft, Delft, Netherlands

<sup>5</sup>Engineering Research Center of Technical Textile, Ministry Education, Shanghai, China

## Corresponding author:

Li Wei, College of Textiles, Donghua University, No. 2999, Northern Renmin Rd, Songjiang District, Shanghai 201620, China.  
Email: [liweid@dhru.edu.cn](mailto:liweid@dhru.edu.cn)

to cracking. Therefore, an integrated jute honeycomb fabric was developed by the three-dimensional (3D) braiding method,<sup>10,11</sup> then a jute/epoxy composite honeycomb manufactured via vacuum assisted resin infusion (VARI).<sup>12,13</sup>

Over the past few decades, a significant number of researchers have investigated the honeycomb structures using theoretical, experimental, and numerical simulation methods. The typical compression behavior of honeycomb structures is as follows: first is the buckling of the cell walls, then the folding of the cells develops, the amount of folding increases and eventually extends over the entire height of the cells, finally is the “densification.”<sup>5</sup> Compressive buckling and crushing are the dominating failure modes for this CFRP honeycomb. For FRCH, in addition to the overall shear-type mode, it also has the failure mode of fiber-reinforced polymer (FRP), such as fiber breakage, fibers pull-out, matrix crack, matrix and fiber debonding, yarn pull-out, etc.<sup>6,14,15</sup> For 3D braiding composites, it was found that the influence of the braided angle was more significant than that of temperature. The failure modes of 3D braided composites with large braided angle were mainly in the forms of resin crack, delamination, and fiber-matrix interface debonding, while that of the smaller braided angle is mainly in the forms of resin cracks and yarn breakage. In addition, the decrease of temperature made the composite more brittle and easier to compressive damage. The yarn fracture mainly occurred in the regions where the braided yarns were in bended and distorted state.<sup>16</sup> As this is a newly developed 3D braided composite honeycomb, its performance and failure mode are not clear, so it is necessary to analyze and study its mechanical behavior and failure mechanisms.

Generally, honeycombs are stiffest and strongest under out-of-plane loading (along longitudinal cell axes), because the cell walls are subjected only to axial stresses; in-plane loading potentially subjects the cell walls to compression/extension and bending failure. For this reason, mechanical properties for in-plane loading (transverse to cell axes) of honeycombs are thought to be most application-limiting, including elastic stiffness and phenomena of elastic buckling and initial yielding that serve as precursors to plastic buckling/collapse.<sup>17,18</sup> Hence, it is important to investigate the in-plane mechanical behaviors of 3D braided jute/epoxy composite honeycombs.

The relative density, the properties of the material, and the geometric characteristics (such as the shape of the cell, the thickness of the cell walls, and so on.) greatly affect the effective mechanical behavior of the honeycomb.<sup>19,20</sup> The mechanical response of honeycomb is an important feature for the optimal design of honeycomb structures. A better understanding of the effect of the geometrical characteristics on the in-plane mechanical behavior is required to improve the design of such materials. A major objective of the current study is to focus on the effect of both loading direction and geometry, more specifically hexagonal joint wall length, on the in-plane compressive properties of the 3D braided jute/epoxy composite honeycombs. In-plane compression was conducted from two transverse directions. Experiment results

were analyzed from compression curves, energy calculation, failure sequence, and failure modes.

In brief, integrated composite honeycomb structures were realized through VARI. Honeycomb fabrics were manufactured with 3D braiding. The novelty of current study is that the influence of geometrical dimensions like the joint wall length on the in-plane compression properties were experimentally evaluated, providing insight into the interplay between material constituents and braided composite honeycomb architectures.

## Materials and fabrication

### Samples description

Three-dimensional (3D) braided honeycomb fabrics were realized on the self-made 3D braiding set-up using jute yarns, as shown in Figure 1. Based on the principle of the 3D braiding “four-step” method,<sup>11</sup> the interlaced state of yarns can be changed by controlling the movement of yarn carriers, so the separation and combination of the braid can be controlled, then 3D braided honeycomb fabrics can be formed. The braiding process and parameter analysis of 3D braided honeycomb fabrics has been described in detail in the published paper.<sup>21</sup> Three types of honeycomb fabrics are molded by VARI to manufacture composite honeycombs. The parameter diagram of the 3D braided honeycomb composite is shown in Figure 2. The dimension of the braided composite honeycomb along the  $X/Y/Z$  direction is defined as width  $W$ , length  $L$ , and height  $H$ , respectively. The hexagonal wall thickness and wall length of the 3D braided honeycomb composite are defined as  $t$  and  $l$ , respectively. The hypotenuse of the hexagonal cell is defined as the free wall, named  $l_1$ , and the vertical wall is defined as the joint wall, named  $l_2$ . The number of braiding cycles for the free wall length  $l_1$  and joint wall length  $l_2$  is  $f_1$  and  $f_2$ , respectively. The angle between two connected free walls is defined as the opening angle  $\delta$ .

The free wall length  $l_1$  and opening angle  $\delta$  of these three types of honeycombs are the same; however, the joint wall length  $l_2$  varies. The opening angle of all samples is  $120^\circ$ . The number of braiding cycles for all samples is 24. For given braiding cycles, the longer joint wall length yields a larger cell size and consequently a smaller cell number. In-plane compression was conducted from two transverse directions, namely,  $X$ , and  $Y$  directions. The  $X$  direction and  $Y$  direction here correspond to  $X$ -axis and  $Y$ -axis in the coordinate system of Figure 2. All manufactured samples are shown in Figure 3. The number of braiding cycles for each type of samples is shown in Table 1.

### Material properties

Jute yarns are commercial product with an average diameter of 2 mm. The matrix is 2511-1A epoxy resin from Shangwei

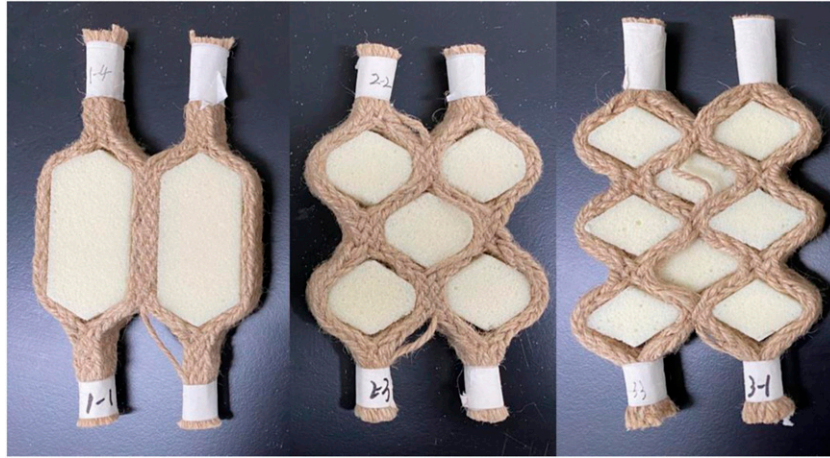


**Figure 1.** 3D braided honeycomb fabrics.

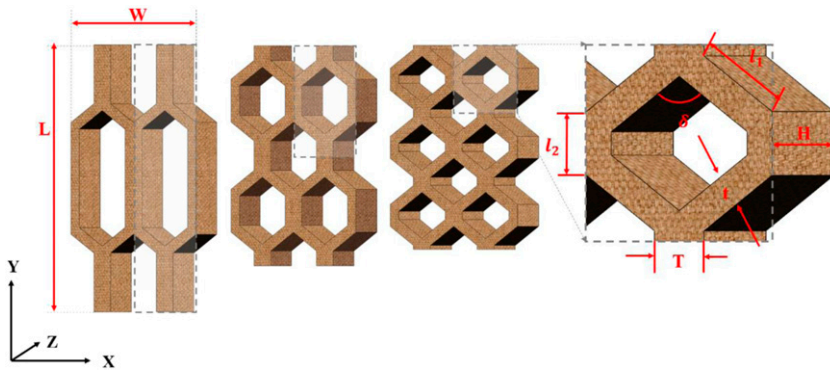


**Figure 2.** The parameter diagram of the 3D braided composite honeycomb.

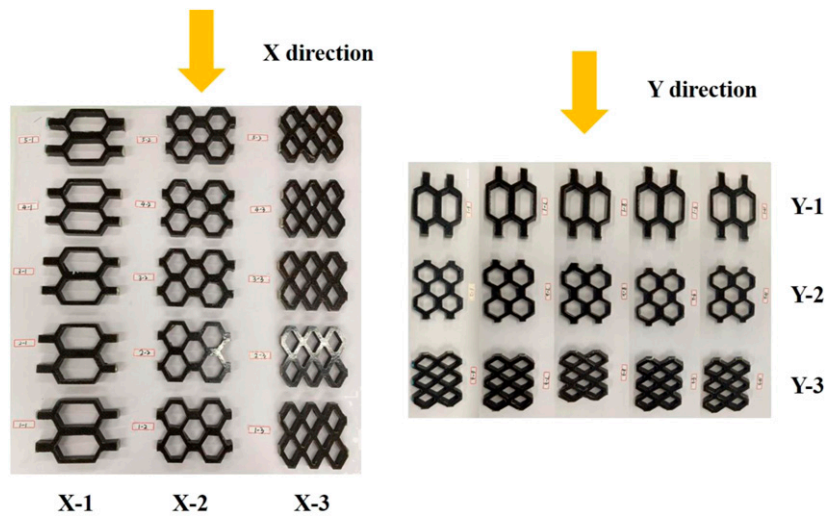


**Figure 3.** The samples of in-plane compression (X/Y-n indicates the sample with  $n$  columns/rows of cells compressed along the X/Y direction).







**Table 1.** The number of braiding cycles for these three types of samples.

	The number of braiding cycles of a unit cell		
	X/Y-1	X/Y-2	X/Y-3
$\frac{f_2}{2}$	5	2	1
$f_1$	2	2	2
$f_2$	10	4	2
$f_1$	2	2	2
$\frac{f_2}{2}$	5	2	1
Number of repeating units	1	2	3
Total number of braiding cycles	24	24	24

**Table 2.** Parameters of epoxy resin.

Density		Tensile strength (MPa)	Tensile modulus (MPa)	Extensibility (%)	Flexural strength (MPa)	Flexural modulus (MPa)
Swancor 2511-IA	Swancor 2511-IBS					
1.1–1.2	0.9–1.0	67–80	2700–3500	4.5–8.5	110–140	2800–3600

**Table 3.** The basic parameters of the samples.

Samples	Illustration	Weight (g) ( ± SD)	Density (g/cm <sup>3</sup> ) ( ± SD)	Fiber mass fraction (%) ( ± SD)	Fiber volume fraction (%) ( ± SD)	Relative density ( ± SD)
C-120°-X-1		69.45 ( ± 4.76)	1.24 ( ± 0.10)	34.87 ( ± 0.83)	29.02 ( ± 5.10)	0.3204 ( ± 0.0356)
C-120°-X-2		76.96 ( ± 5.96)	1.24 ( ± 0.12)	33.29 ( ± 1.58)	27.48 ( ± 7.74)	0.3761 ( ± 0.0404)
C-120°-X-3		77.96 ( ± 4.30)	1.19 ( ± 0.08)	32.80 ( ± 1.63)	29.62 ( ± 5.95)	0.4582 ( ± 0.0371)
C-120°-Y-1		74.14 ( ± 1.46)	1.19 ( ± 0.08)	33.96 ( ± 0.64)	30.84 ( ± 4.34)	0.3403 ( ± 0.0222)
C-120°-Y-2		75.44 ( ± 1.58)	1.23 ( ± 0.11)	32.33 ( ± 1.22)	26.71 ( ± 7.73)	0.3713 ( ± 0.0350)
C-120°-Y-3		77.18 ( ± 3.81)	1.26 ( ± 0.08)	32.92 ( ± 0.89)	25.68 ( ± 4.39)	0.4283 ( ± 0.0290)

Comments: Standard Deviation (SD).

(Tianjin) Wind Power Materials Co., Ltd., and the curing agent is 2511-IBS. The mass ratio of the matrix and the curing agent is 100:30. Hardening conditions: After the sample is cured at room temperature (28°C) for 24 hours, it is post-hardened at 70°C for 8 hours. The mechanical properties of the utilized epoxy resin are listed in Table 2. The basic geometrical parameters of the honeycomb samples, as well as the fiber volume fraction of the composites, and the overall honeycomb density are summarized in Table 3. As the joint wall length decreases, the relative density will increase slightly.

### Experimental set-up

The in-plane compression testing was performed on a LAB-SANS LD26 electro-hydraulic servo universal testing machine with a max range of 100 kN. The speed of loading is 2 mm/min. At the same time, 3D - DIC (Digital Image Correlation) measuring system of Correlated Solutions Company is used to record the full field strain of 3D braided composite honeycomb during in-plane compression. A photographic image and a schematic diagram of the experimental equipment are shown in Figure 4.



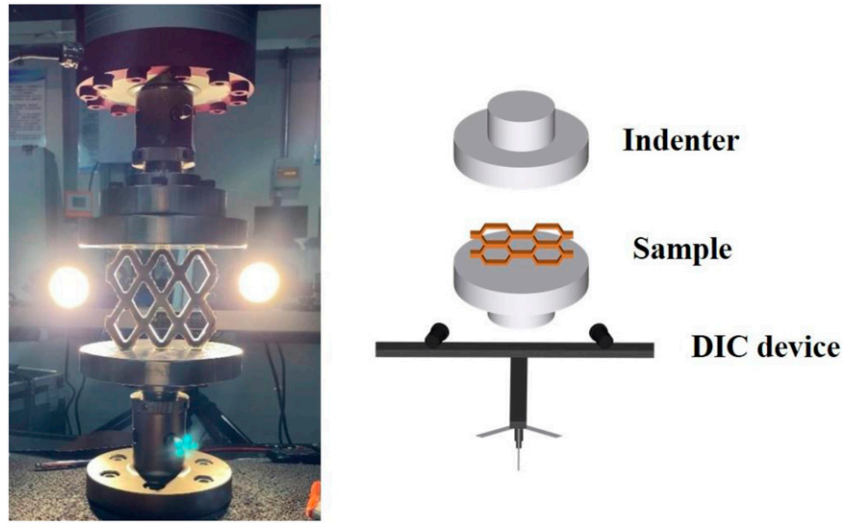


**Figure 4.** A photographic image and a schematic diagram of the experimental compression equipment.

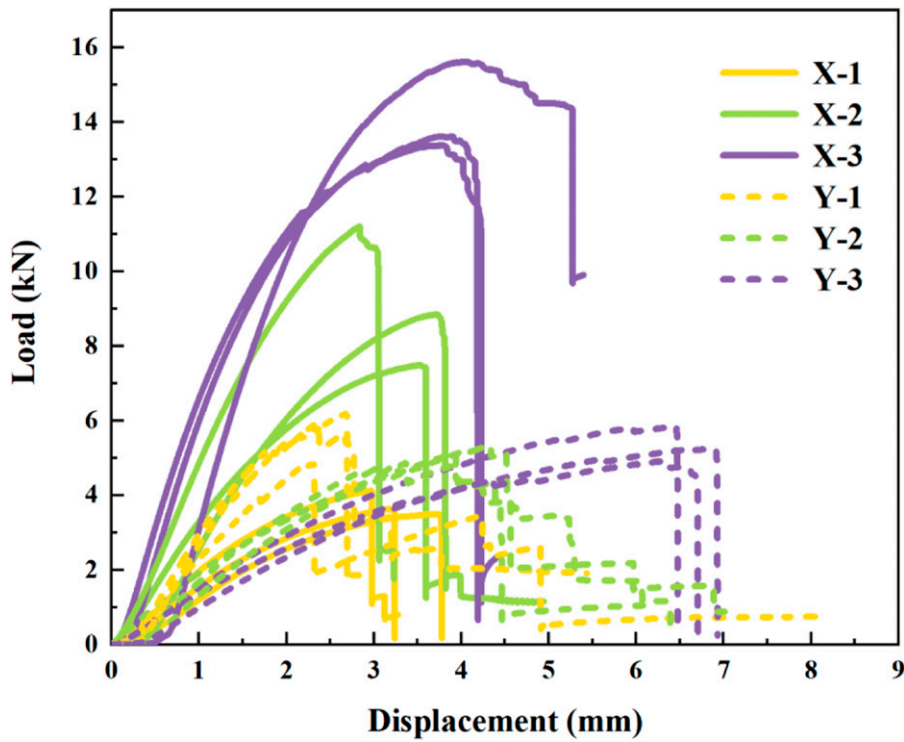


**Figure 5.** The load-displacement curves of all samples.

## Results and discussion

### *In-plane compression curve*

Generally, when honeycombs made of ductile materials are compressed, there will be three stages on the load-displacement curves: the initial stage is the linear elastic stage, followed by the plateau stage and finally the steep

“densification” stage. Before reaching the critical stress, the stress increases linearly with the increase of strain, which forms an initial linear region. When plastic hinges develop on the inclined walls, the linear elastic behavior ends, and the plateau stage starts. The stage called densification is located after the plateau stage. In the densification stage, the stress increases rapidly. Although this explains the general compression behavior of honeycomb crushing, changes in

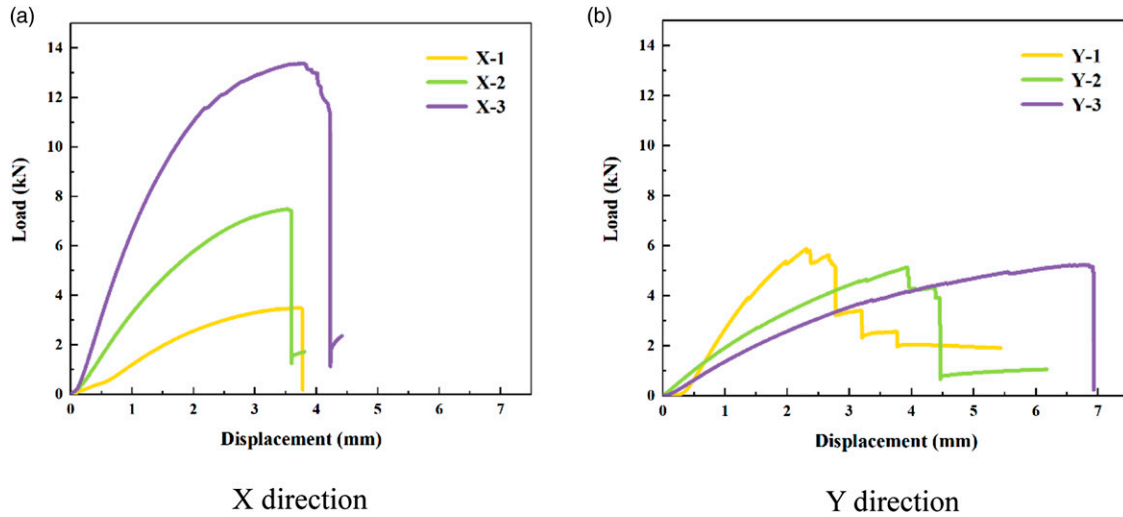


**Figure 6.** The load-displacement curves of representative samples.

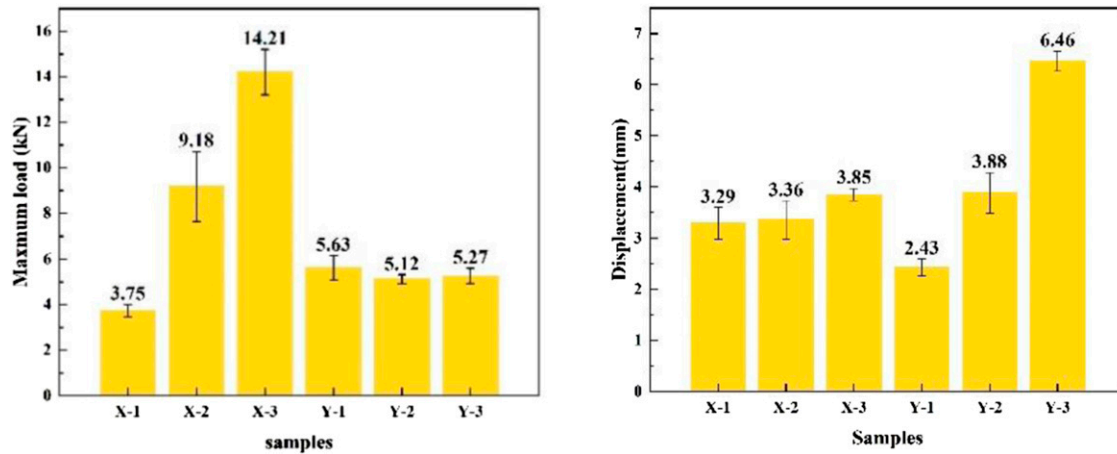


**Figure 7.** The maximum load and displacement corresponding to the maximum load of samples.

material properties and geometric parameters can lead to differences.<sup>22</sup>

The curves of all samples are shown in Figure 5, and select representative curves of samples for detailed comparison and analysis, as shown in Figure 6. The load-displacement curves of 3D braided honeycomb structures studied in this paper can be divided into two stages: The first stage is that the load increases with the increase of displacement. At the initial stage of loading, the load changes linearly with the change of displacement, the samples are in the elastic deformation stage. At this stage, the combination of resin and fiber is good, so the slope of the curve increases rapidly. Then, the load continues to increase, the sample begins to deform, the resin matrix cracks, and the material surface cracks. At this time, a slight cracking sound of the matrix can be heard. However, with the further increase of the load, the ultimate

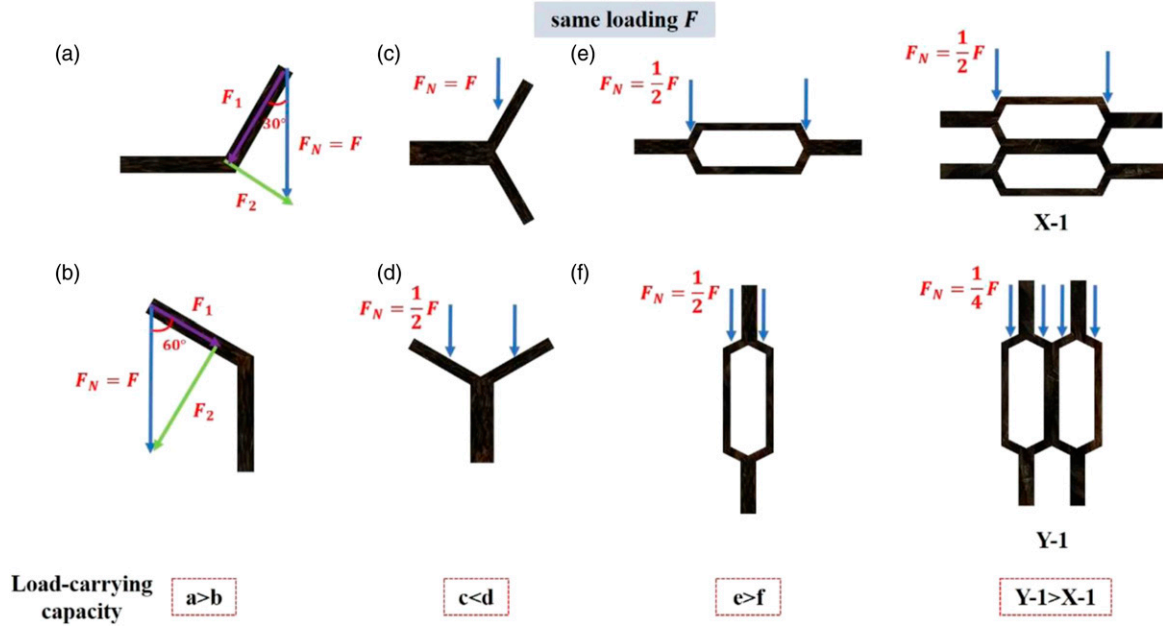
bearing capacity of samples is reached, that is, at the maximum load. The second stage is that the load decreases with the increase of displacement: one is “cliff type” descent, the other is “ladder type” descent, which will be discussed in detail later in this paper. The compression performance of 3D braided honeycombs studied in this paper is obviously different from that of the honeycombs with three typical stages, and there is no plateau area and densification stage. This is related to the ratio of wall thickness to wall length and the relative density of honeycomb structures. The wall thickness of the honeycomb structure studied in this paper is thick. When bearing load, the free wall is equivalent to a column rather than a beam. It will not be bended, and it will show brittle fracture at the node, so it will not show plateau stage and densification stage. The relative density of samples in this study is relatively high. When the relative density of honeycomb



**Table 4.** Geometrical and compressive strength data of the honeycombs.

Core type	Fabrication technique	Wall thickness $t$ (mm)	Core height $H$ (mm)	Density (kg/m <sup>3</sup> )	Compressive strength (MPa)
Jute/VE honeycomb core <sup>5</sup>	Hot press molding	1.43	10	290	14.99
Jute/epoxy Honeycomb X-1	VARI	1.11	10	157	13.48
Jute/epoxy Honeycomb X-2		6.69	15	1239	15.3
Jute/epoxy Honeycomb X-3		6.70	15	1194	31.57
Nomex honeycomb <sup>24</sup>	Commercial	0.051	12.7	32	0.01
			12.7	48	0.02
		0.076	12.7	50	0.04
			25.4	96	0.18
Pure PLA	3D printed	1.5	10.5	460	4.07
Reinforced Al alloy <sup>25</sup>				560	7.65
				1060	18.95

(Note: Compressive strength of 3D braided composite honeycomb = maximum load ÷ contact area between honeycomb and indenter.).

**Figure 8.** The diagram of force analysis.

exceeds 0.3, the cell walls are too short and stocky to buckle.<sup>23</sup>

When the load is applied along  $X$  direction, the load-displacement curves show a “cliff-like” decline, which corresponds to a sudden brittle failure, as shown in Figure 6(a). When the load is applied along  $Y$  direction, the curves of Y-1 and Y-2 show a “stepped” descent after

reaching the maximum load, showing a trend of progressive damage, while the curve of Y-3 did not show a progressive failure process and eventually collapsed due to brittle fracture, as shown in Figure 6(b). When the load is applied along  $X$ -direction, as the joint wall length decreases, the maximum load increases gradually, that is,  $X-1 < X-2 < X-3$ . When the load is applied along  $Y$  direction, there is not much

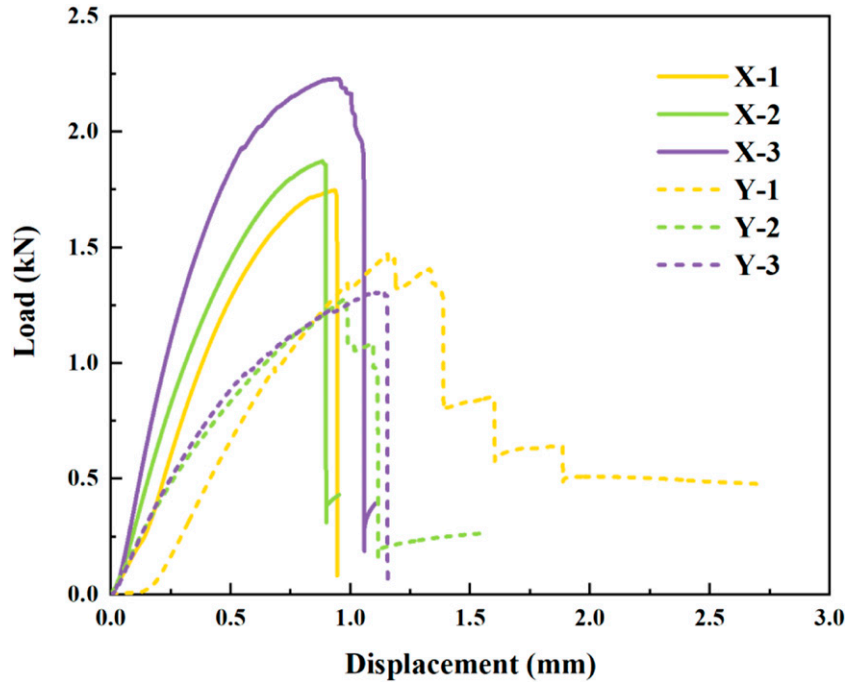


**Figure 9.** The normalized load-displacement curve of representative samples.

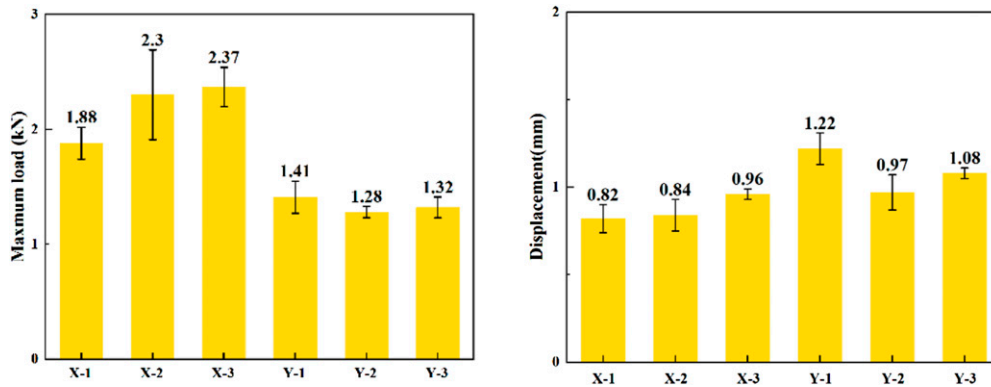


**Figure 10.** The normalized maximum load and displacement corresponding to maximum load of samples.

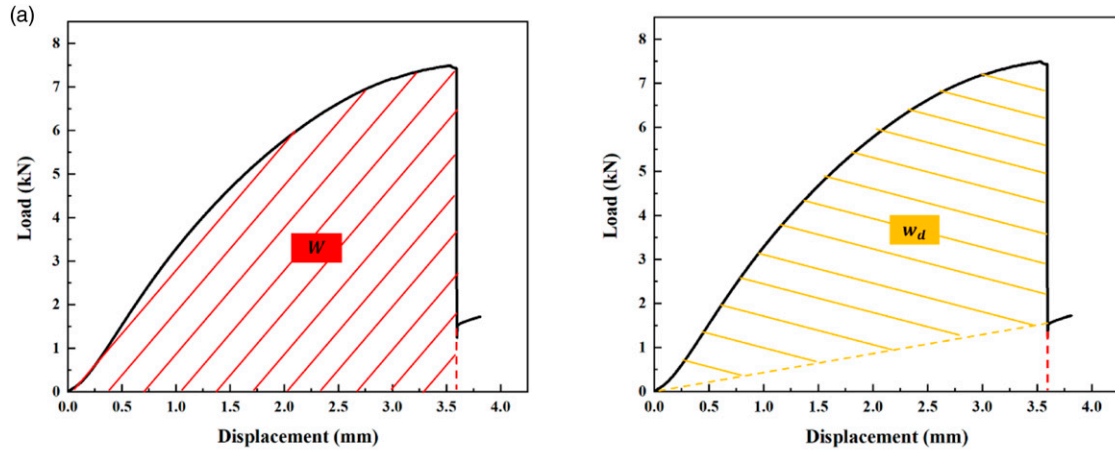
**Table 5.** Energy value of representative samples.

Sample	$w_d/W$				
	1	2	3	4	5
X-1					0.96
X-2					0.81
X-3					0.87
Y-1	0.13	0.47	0.37	0.28	0.26
Y-2			0.29	0.18	0.84
Y-3					0.96

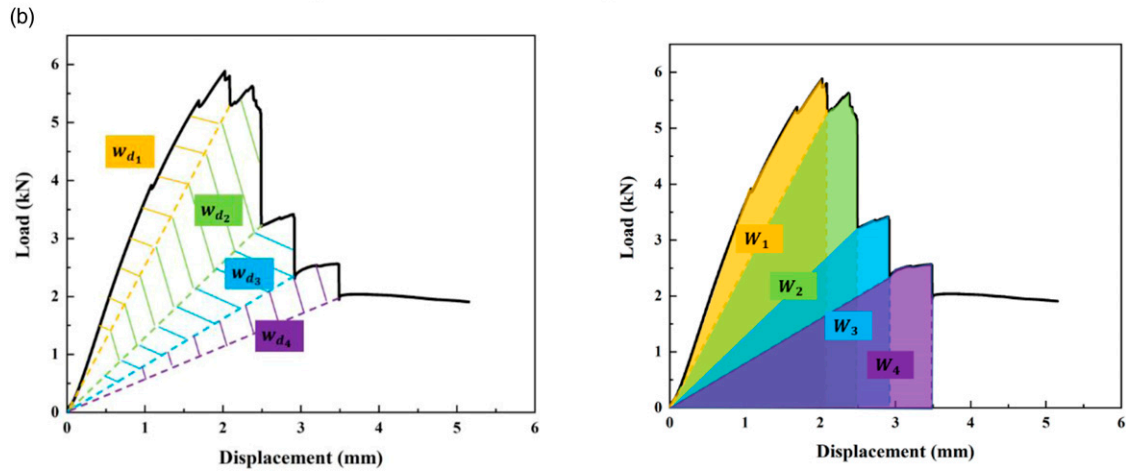
difference in maximum load, but a clear difference in displacement corresponding to maximum load, that is,  $Y-1 < Y-2 < Y-3$ . The maximum load and displacement

corresponding to maximum load of samples are shown in Figure 7. The currently developed 3D braided composite honeycombs yield to higher density with other honeycombs, as shown in Table 4. However, the compressive strength in both directions seem to outperform most commercially available honeycombs as summarized in Table 4. Nonetheless, the current 3D braided composite honeycomb needs further optimization of their density. With the same number of braiding cycles, the shorter the joint wall length and higher number of cells lead to higher load-weight efficiency.

The maximum load of samples tested in  $X$  direction increases and can be explained by that X-1 has two columns of free walls, X-2 has four columns of free walls, and X-3



load-displacement curves of samples exhibit 'cliff-like' descents



Load-displacement curves of samples exhibit 'ladder type' descents.

**Figure 11.** Relationship between load-displacement and energy ( $W$  is the total work applied to the samples with the area underneath the load-displacement curve.  $w_d$  is the energy dissipated with fracture, enclosed by the curve and the remaining stiffness).

has six columns of free walls. When load is applied along  $X$  direction, the free walls carry all load. The joint wall is perpendicular to the loading direction and does not contribute to carrying load. Therefore, when the number of columns increases, the maximum load is higher. Transverse to that, Y-1, Y-2, and Y-3 all have four columns of free walls, they have the same load-carrying capacity. Therefore, when the force is loaded in the  $Y$ -direction, the maximum load is nearly the same. The load-carrying capacity of samples is also related to the angle between the free wall and the loading direction. When the load  $F_N$  is applied to one free wall in X-1 and Y-1,  $F_N$  can be decomposed into a force  $F_1$  parallel to the free wall and a force  $F_2$  perpendicular to the free wall, as shown in Figure 8(a) and (b). So  $F_2$  is the key to the failure of samples. The angle between the free wall and the loading direction is bigger when the same load is applied to one free wall, the force  $F_2$  is larger, then the free wall is

easier to be damaged. For X-2 and Y-2, they have a similar configuration in the number of cell rows and cell columns, but the maximum load of X-2 is larger. This is because the angle between the free wall and the loading direction is smaller when the load is applied in  $X$  direction.

When a free wall is added vertically, the load is transmitted in the longitudinal direction, and the load that every free wall bears remains unchanged, as shown in Figure 8(a)–(c). But adding a free wall horizontally will share half of the force as shown in Figure 8(b)–(d), so (c) is more likely to be damaged. The number of free wall columns in (e) and (f) is the same, but the load-carrying performance of (e) is better because the angle between the free wall and loading direction of (e) is smaller. Increasing the number of free wall rows will not share the load, so the maximum load of Y-1 is greater than that of X-1. There are four free walls in the longitudinal direction for X-2 and Y-1, but the load-bearing

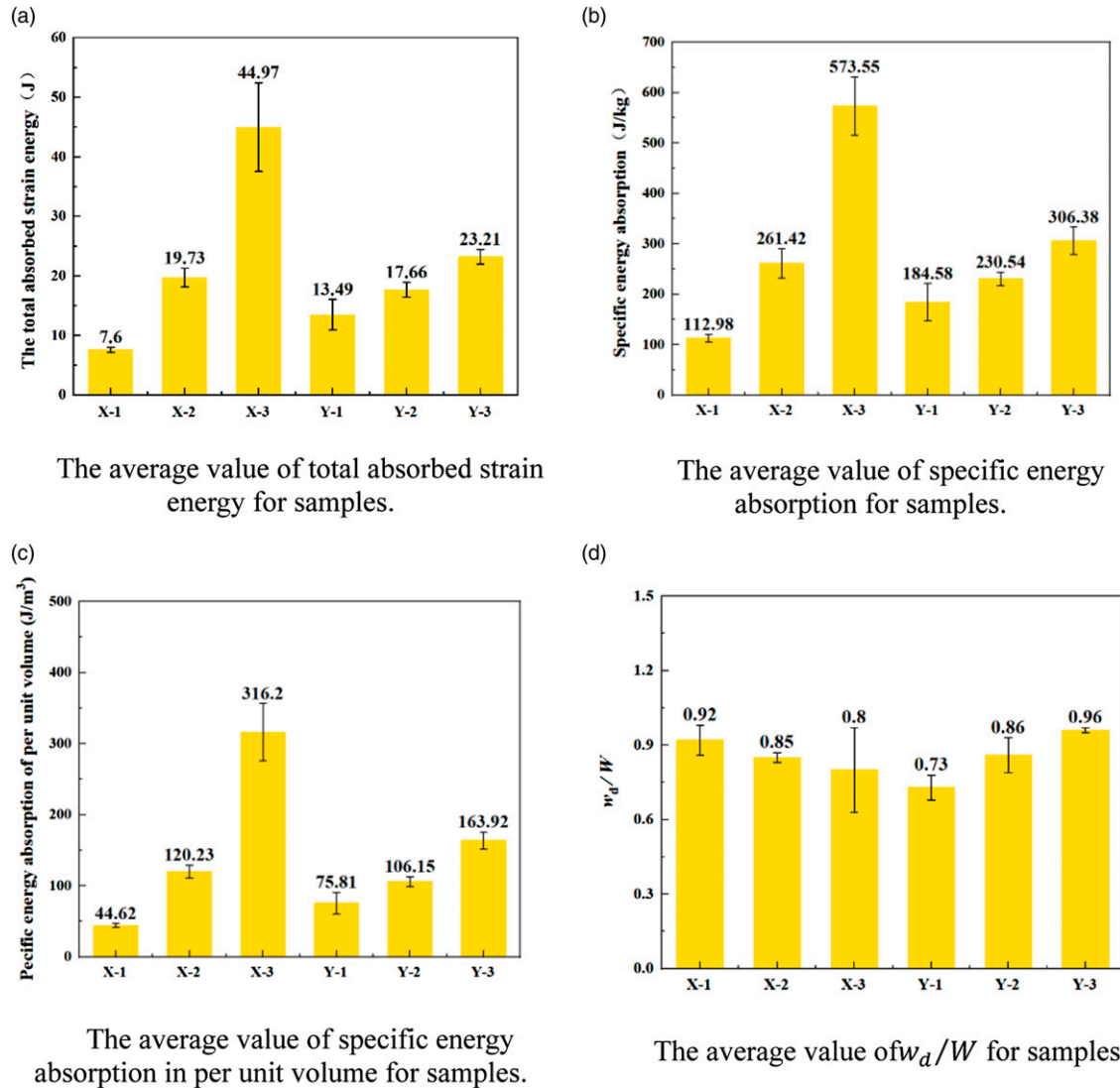


**Figure 12.** The average value about energy of samples.

capacity of X-2 is greater than that of Y-1 because the angle between the free wall and the loading direction of X-2 is bigger. Similarly, the bearing performance of X-3 is greater than that of X-2 due to it having more free wall columns. To sum up, the comparison of the maximum load of the sample is  $X-3 > X-2 > Y-1 \approx Y-2 \approx Y-3 > X-1$ .

The opposite seems true when looking at the displacement. This can be explained by that X-1, X-2, and X-3 all have two rows of hexagonal cells and four rows of free walls. But Y-1 has one row, Y-2 has two rows, while Y-3 has three rows of hexagonal cells, and they have two rows, four rows, and six rows of free walls, respectively. Therefore, the more rows of unit cells, that is, the more rows of free walls, the displacement corresponding to the maximum load is greater.

To illustrate the above-described relationships, the load-displacement curves can be normalized with respect to the

identified contributing elements. That is, divide the maximum load of the sample by the number of their free wall columns, and the displacement corresponding to the maximum load of the sample by the number of their free wall rows. The maximum load of X-3 and X-2 is 3.8 times and 2.5 times higher than that of X-1, respectively. After normalization, the load capacity of each free wall of X-3 and X-2 is 1.3 and 1.2 times higher than that of X-1, as shown in Figures 9 and 10. This basically conforms to the conclusion that the load capacity of each free wall is basically the same. However, with the increase of the number of cells, the multiple of the maximum load will also increase slightly. This is because different joint wall lengths lead to different number of cells in the same number of braiding cycles, resulting in different relative density of 3D braided composite honeycomb. With the decrease of the joint wall length, the relative density gradually increases, as shown in

Table 3, which is also the factor that causes the enhancement of the mechanical properties of 3D braided composite honeycomb. Just as the normalized maximum load, the maximum load of X-1, X-2, and X-3 also slightly increases. However, the effect of cells' configuration on mechanical properties is greater than that of relative density. Both the honeycombs' relative density and the geometric configuration of cells have an important influence on the mechanical properties of honeycombs. But the respective weights of the two factors depend on the crushing velocity and the loading manners. The influence of the cells' configuration is weakened with the increase of the crushing velocity, while that of the honeycomb's relative density is strengthened.<sup>26</sup> The in-plane compression in this paper belongs to the range of low speed, so the configuration of cell plays a decisive role.

The displacement corresponding to the maximum load of Y-3 and Y-2 is 2.7 times and 1.6 times of Y-1, respectively. After normalization, the displacement under the maximum load of each free wall rows of Y-3 and Y-2 is 0.9 and 0.8 times of Y-1, respectively. This is also basically in line with the fact that the deformation of each row of free wall under the maximum load is the same. However, with the increase of the number of cell rows of Y-2 and Y-3, the deformation of each row of free wall will be slightly smaller than that of Y-1. This is because under the same number of free wall columns that bear the load, the number of free wall

rows continues to increase without increasing the bearing capacity. Although the relative density has increased, it has resulted in more connection points that are prone to fracture (the connection between the joint wall and the free wall), resulting in the instability of the structure.

Therefore, according to the above analysis, increasing the number of unit cell columns will increase the load-bearing properties of 3D braided composite honeycombs, while increasing the number of unit cell rows will increase the displacement corresponding to the maximum load of 3D braided composite honeycombs. In the meantime, the angle between a free wall and the loading direction is smaller, the load-bearing properties of 3D braided honeycomb composites are bigger.

The conclusion of samples with an opening angle of  $120^\circ$  is also verified by the in-plane compression test of samples with an opening angle of  $90^\circ$ . That is, the maximum load of the sample is related to the number of cell columns, while the displacement corresponding to the maximum load is related to the number of cell rows. At the same time, the angle between the free wall and the loading direction will also affect the maximum load of samples. The in-plane compression properties of samples with an opening angle of  $90^\circ$  and the effect of other variables (opening angle, matrix material) on the in-plane compression properties of 3D braided composite honeycombs will be introduced in detail in another paper.

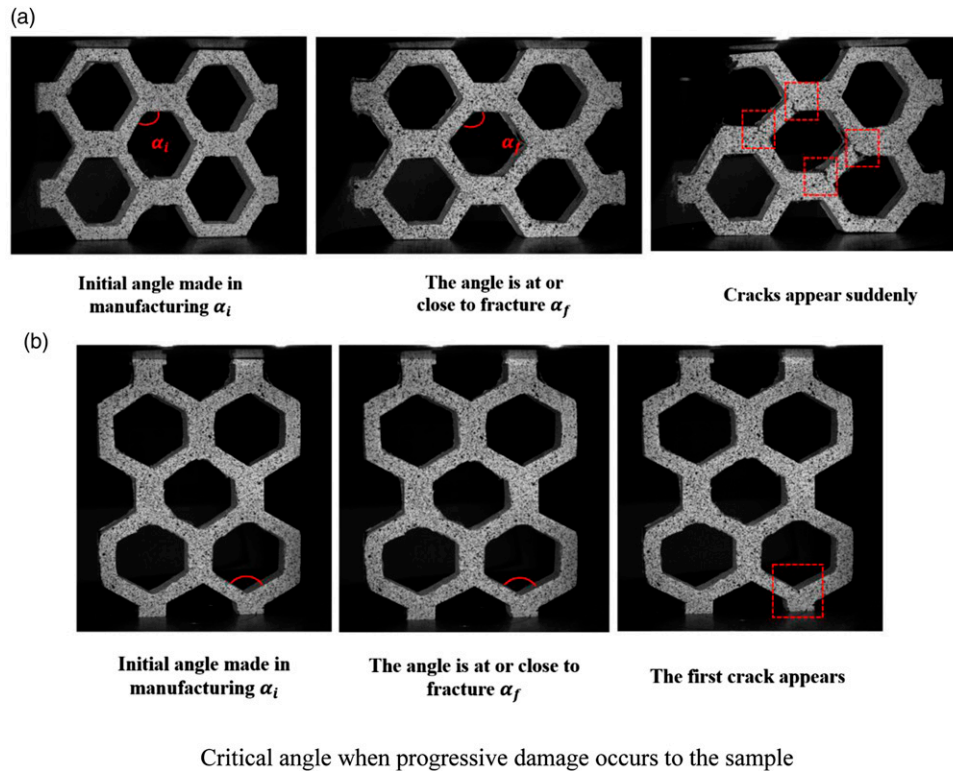


**Figure 13.** Schematic diagram of the failure angle.



### Strain energy evaluation

The total absorbed strain energy, specific energy absorption, and specific energy absorption per unit volume are used to evaluate the strain energy absorption.

The total absorbed energy  $W$ , which describes the energy absorption capacity of every sample, is defined by<sup>27</sup>

$$W = \int_0^s F(u)du \quad (1)$$

where  $F(u)$  is the load as a function of the displacement  $u$ , and  $s$  is the compressive displacement.

The specific energy absorption (SEA), which is defined as the energy absorbed per unit mass, is given by<sup>27</sup>

$$SEA = W/m \quad (2)$$

where  $m$  is the mass of the energy absorber. Similarly, the specific energy absorption per unit volume (SEAv) is the energy absorbed by a structure per unit volume given by

$$SEAv = W/V \quad (3)$$

where  $V$  is the entire honeycomb cuboid structure.<sup>28</sup>

The ratio of the amount dissipated energy  $w_d$  to the corresponding work applied  $W$  is defined as the intrinsic resistance of structures. Resistance to damage formation as a threshold (similar to static friction), then the load needs to exceed a certain level before damage is formed and load drop is visible. Resistance is also the energy it cost to create damage (kinematic friction); then the magnitude of the load drop reflects this resistance. The value of representative samples is shown in Table 5. The lower the ratio, the more intrinsic resistance the material has, the drop of curves is small. When load-displacement curves of samples exhibit “cliff-like” descents, the energy is suddenly released due to the brittle fracture of samples, as illustrated in Figure 11(a). At this time, the value of  $w_d/W$  is high, the resistance of the structure is low, and the drop of curves is large. When load-displacement curves of samples exhibit “ladder type” descents, the crack appears gradually and

each crack will release some energy, as shown in Figure 11(b). And at this time, there are several values of  $w_d/W$ , like Y-1 and Y-2. The  $w_d/W$  of them is small, and their values tend to be constant, the damage will happen when these structures exceed the value. So brittle damage has the tendency to show these significant drops in the curve, while ductile damage goes more progressively by little drops in the curve.

The total absorbed strain energy, specific energy absorption, specific energy absorption per unit volume of samples, and the value of total  $w_d/W$  are shown in Figure 12. The results illustrate that when the load is applied in both directions, the total energy, specific energy, and specific energy absorption per unit volume increase with the increase of the number of cells. When the load is applied along the  $X$  direction, the total absorbed strain energy of X-3 is 5.9 times higher than that of X-1, while the total absorbed strain energy of X-2 is 2.6 times higher than that of X-1. When the load is applied along the  $Y$  direction, the total absorbed strain energy of Y-3 is 1.7 times higher than that of Y-1, and the total absorbed strain energy of Y-2 is 1.3 times higher than that of Y-1.

No matter the load applied along  $X$  direction or  $Y$  direction, the energy absorption performance increases with the decrease of the joint wall length and the increase of the number of cells. This is also similar to the in-plane mechanical properties of aluminum honeycomb.<sup>29,30</sup> When the load is applied along  $X$  direction, with the decrease of the joint wall length and the increase of the unit cell number, the value of  $w_d/W$  decreases, indicating that the total resistance of the material is gradually increasing. However, when the load is loaded along the  $Y$  direction, the value of  $w_d/W$  increases with the increase of the number of cells. The total resistance of the material decreases in turn.

Although the energy absorption of X-2, X-3, and Y-3 are greater than that of Y-1 and Y-2, their energy will be released suddenly due to the brittle fracture, which cannot be used as a good energy absorption structure. Honeycombs with more columns comprising free walls parallel to the loading direction demonstrate higher load-carrying as well as higher

**Table 6.** The crucial angle of samples.

Samples	Failure angle $\Delta\alpha \pm DS$ (°)	Definition of failure angle	Description of the failure process
X-1	$7.16 \pm 1.04$	I	With the decrease of the indenter, a very small crack appears on the sample. With the continuous decrease of the indenter, the crack propagation is not obvious until the sample suddenly cracks
X-2	$6.77 \pm 1.31$	I	First of all, cracks are produced at the cutting end, and small cracks are gradually produced on samples, and finally suddenly collapse
X-3	$5.48 \pm 0.66$	I	
Y-1	$4.5 \pm 0.59$	II	Cracks on the sample are generated in turn and gradually expand to form large cracks
Y-2	$5.27 \pm 0.65$	II	Cracks are generated in turn, gradually expand, and then suddenly collapse
Y-3	$5.9 \pm 1.49$	II	

(Note: I, II in the table correspond to the two definitions of the above critical angle).



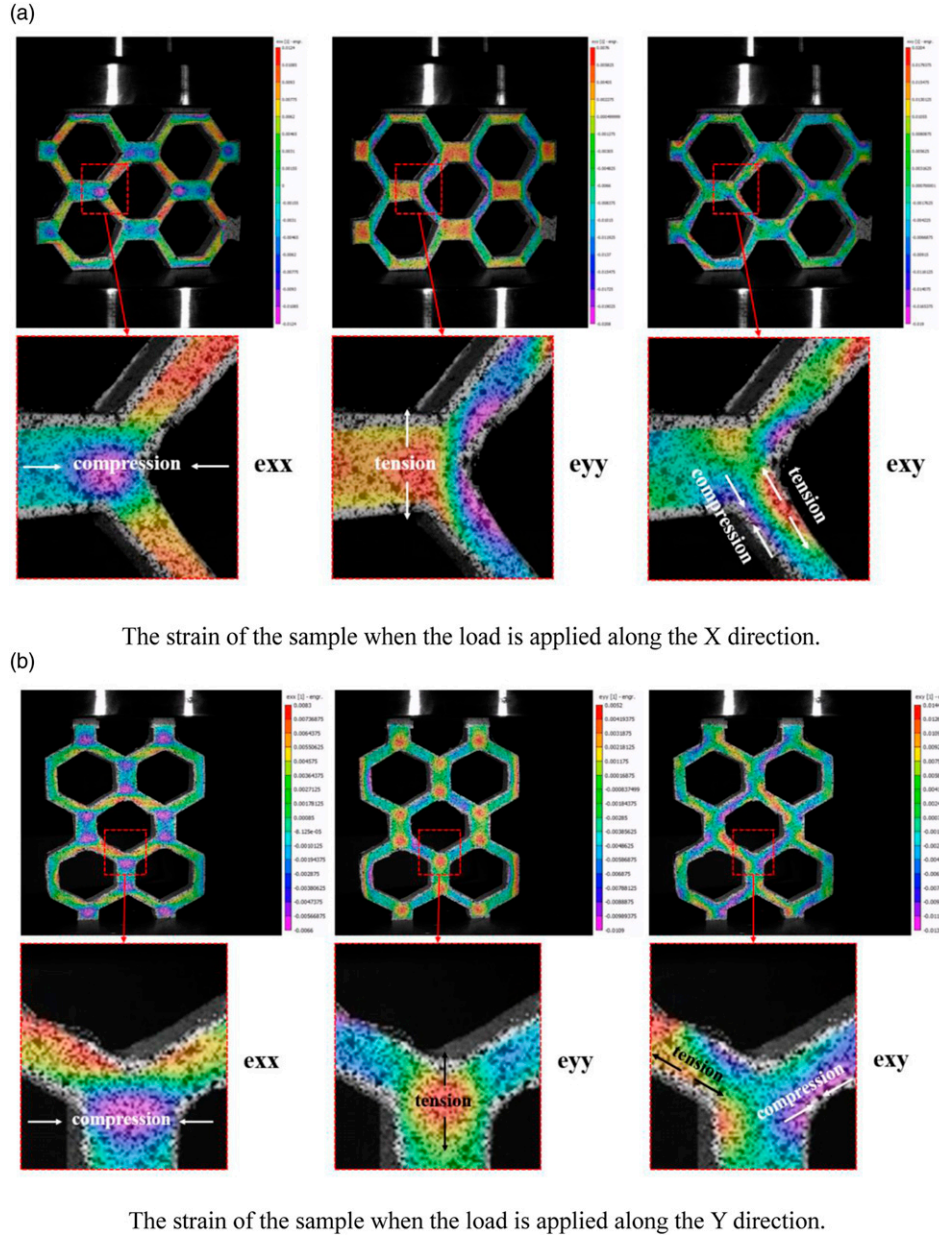


**Figure 14.** Strain of samples observed by DIC.

energy absorption capabilities. Decreasing the joint wall length increases the energy absorption per unit mass and energy absorption per unit volume. It is also shown that a cell shape like a diamond, where the joint walls disappear, is not suitable for energy absorption.

### The process of failure

In the process of loading, the magnitude of the angle reflects the maximum deformation that can occur to the samples prior to failure, that is, the critical deformation. This deformation is also crucial for evaluating the mechanical

properties of samples. Therefore, this paper uses the failure angle to represent the critical deformation of the samples. The angle  $\alpha_i$  is the initial angle made in manufacturing,  $\alpha_f$  is the angle at or close to fracture, and  $\Delta\alpha = \alpha_f - \alpha_i$  is the failure angle, that is, critical angle. There are two conditions for the definition of critical angle, namely, (I) The sample presents brittle fracture, and there is no obvious crack before the sudden and large number of cracks occur at the same time, as shown in Figure 13(a), take the average value of the corresponding angles at the moment before these cracks appear. (II) The sample shows progressive damage, and cracks appear in turn. At this time, the first crack is used to

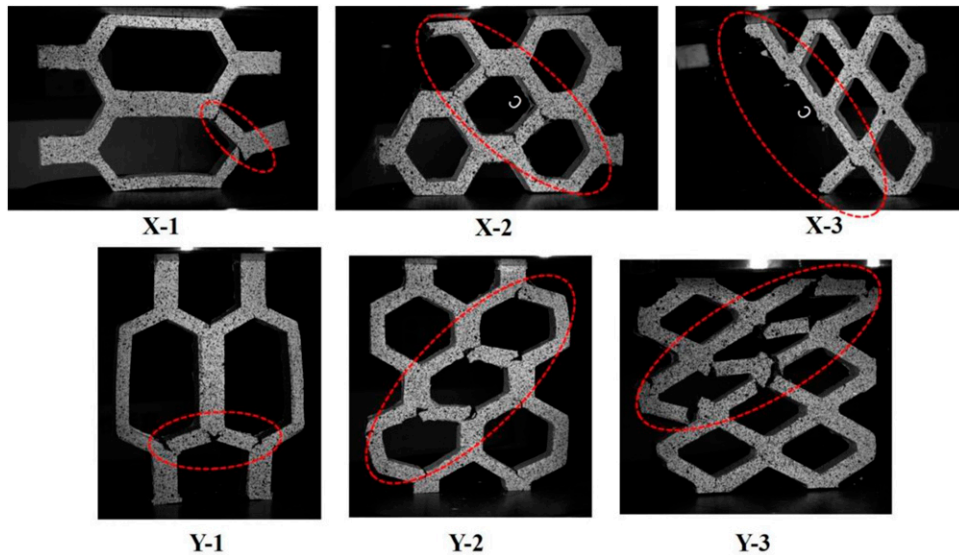


**Figure 15.** Shear failure of the samples.

calculate the fracture angle, as shown in Figure 13(b). Even if the cracks of some samples first break at the cutting end, the critical angle is still defined when the cell wall of samples cracks. The failure angle and its average value are shown in Table 6. When the load is applied along  $X$  direction, with the decrease of the joint wall length, the critical angle becomes smaller and smaller, indicating that the specimen is less likely to deform and the stiffness is greater. When the load is applied along the  $Y$  direction, with the decrease of the joint wall length, the critical angle becomes larger and larger, and the sample can be destroyed only after greater deformation, while the stiffness is gradually reduced. The size of the failure angle also corresponds to the slope of the initial straight section of the load-displacement curves in Figure 6.

The failure angle is about 4 degrees–7 degrees. The failure angle shows that the damage deformation of the samples is about 5%. If it is to be used as an energy absorbing element, it is necessary to improve the deformability of the material and reduce the occurrence of brittle fracture. Maybe a more ductile epoxy matrix with higher fracture toughness can be used to improve energy absorption performance.

### Analysis of failure modes

When a 3D braided honeycomb is compressed, the cell walls deform elastically at first. The load is transmitted through the honeycomb struts as a set of discrete forces and moments acting on cell walls. Because the ratio of length to thickness of the cell wall is too large, consequently, the relative density of the honeycomb is too big, a cell wall is now similar to a column rather than a beam, so plastic

bending will not occur in the honeycomb. And there will be no folding and contact in the honeycomb cell wall. The honeycomb cell wall will only buckle slightly, and directly break at the plastic hinge. When the breaking strength of the cell wall is exceeded, the crack propagates. Crack spreads from the cell to the neighboring diagonal cell that has been weakened and destabilize.<sup>31</sup>

Regardless of whether the sample is loaded in  $X$  direction or  $Y$  direction, the “ $Y$ ” conjunction (the red dashed box in Figure 13) is compressed in the  $Y$  direction and stretched in the  $X$  direction. Therefore, at the junction of joint wall and free wall, the forces on both sides are opposite, one side is under tension and the other side is under compressure, resulting in the overall shear force of samples, these can be seen from DIC, as shown in Figure 14.

If there is no imperfection on the geometry, the crushing is uniform which means that the vertical walls do not tilt but compress. Experiments show that in a real case, the crushing is not actually uniform, the vertical walls tilt because there will always be some imperfections in the manufacturing process.<sup>22</sup> All samples displayed a shear-type instability of the cells. These fractures occur mostly in cells along the inclined band of collapsing cells, as shown in Figure 15. This is similar to the behavior of some conventional metallic honeycomb,<sup>26</sup> Nomex honeycomb,<sup>32</sup> and 3D-printed honeycomb.<sup>33</sup> In the case of aluminum honeycombs, the walls deform plastically while folding. On the other hand, the folding of the Nomex, which is relatively brittle compared to aluminum, results in fractures in the cell walls. In both cases, the number of folding increases and eventually extends over the entire height of the cells. But in contrast to the Nomex and aluminum, the jute/epoxy do not suffer from the unstable failure due to buckling of the cell

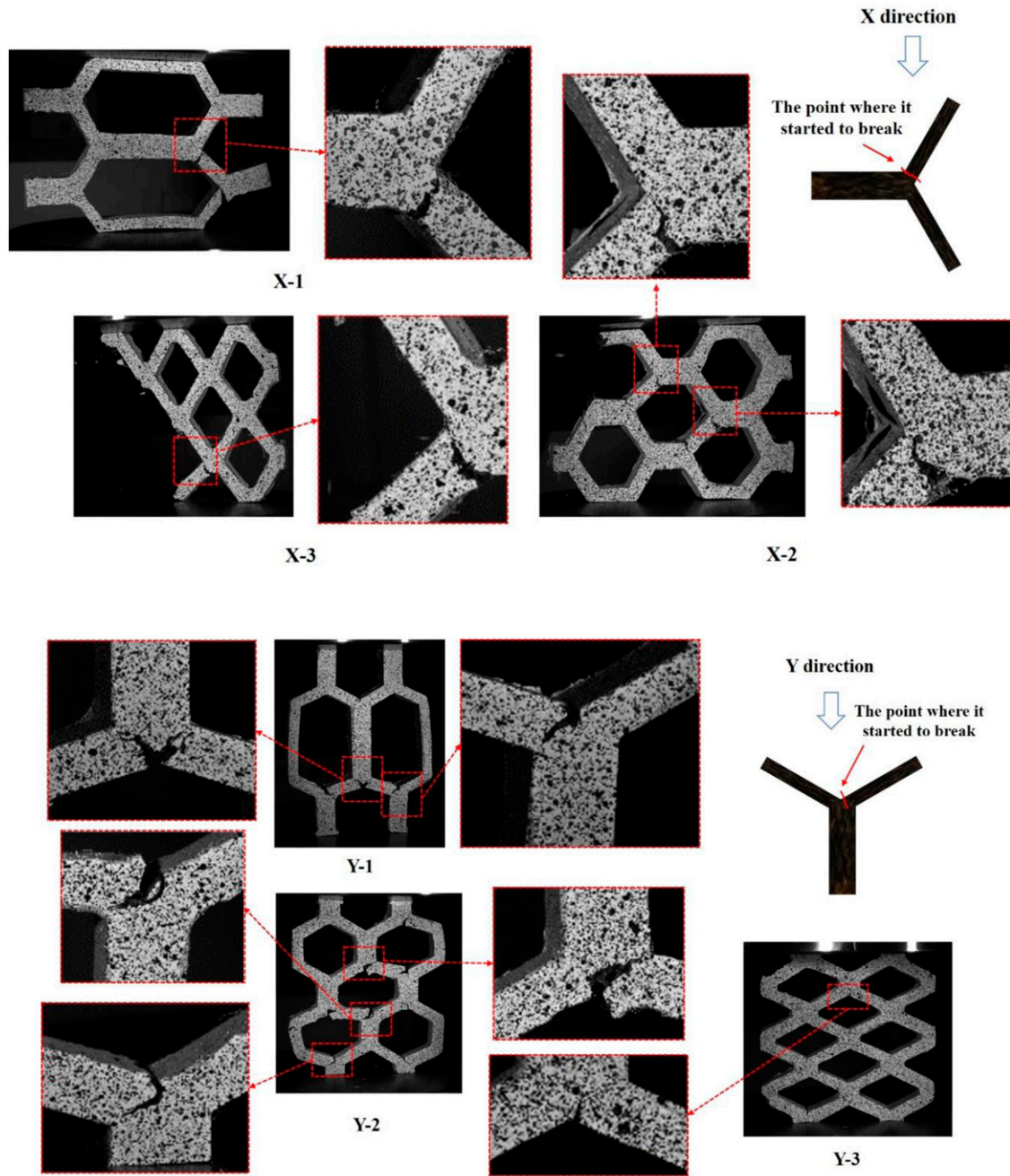


**Figure 16.** Analysis of failure position (The cracks all propagate from the junction of the free wall and the bonded wall.).

walls, but a damage due to typical fiber-composite failure mechanisms.<sup>5</sup> All cracks occur at the interface between the free wall and the joint wall, as shown in Figure 16. Select one of fracture section for failure mechanism analysis, as shown in Figure 17. In particular, the micrograph in Figure 17(a) shows a typical yarn pull-out, while closer view in Figure 17(b) showing the fiber breakage, matrix breakage, and fiber-matrix debonding. Figure 17(c) and (d) captures the fiber pull-out. In addition, in Figure 17(c) and (d), the broken

yarn bundles at four different directions are present, which corresponds to the microstructure of the braided yarn<sup>11</sup> and its cross-sectional shape<sup>34</sup> in the 3D braided composites.

When the load is applied in *X*- direction, it is always brittle because there is no vertical wall to bear the load. The joint wall is perpendicular to the direction of the load and is not subject to force. At this time, it is the free wall that bears the load. All free walls are stressed almost simultaneously, and thus, fracture occurs at the same time.



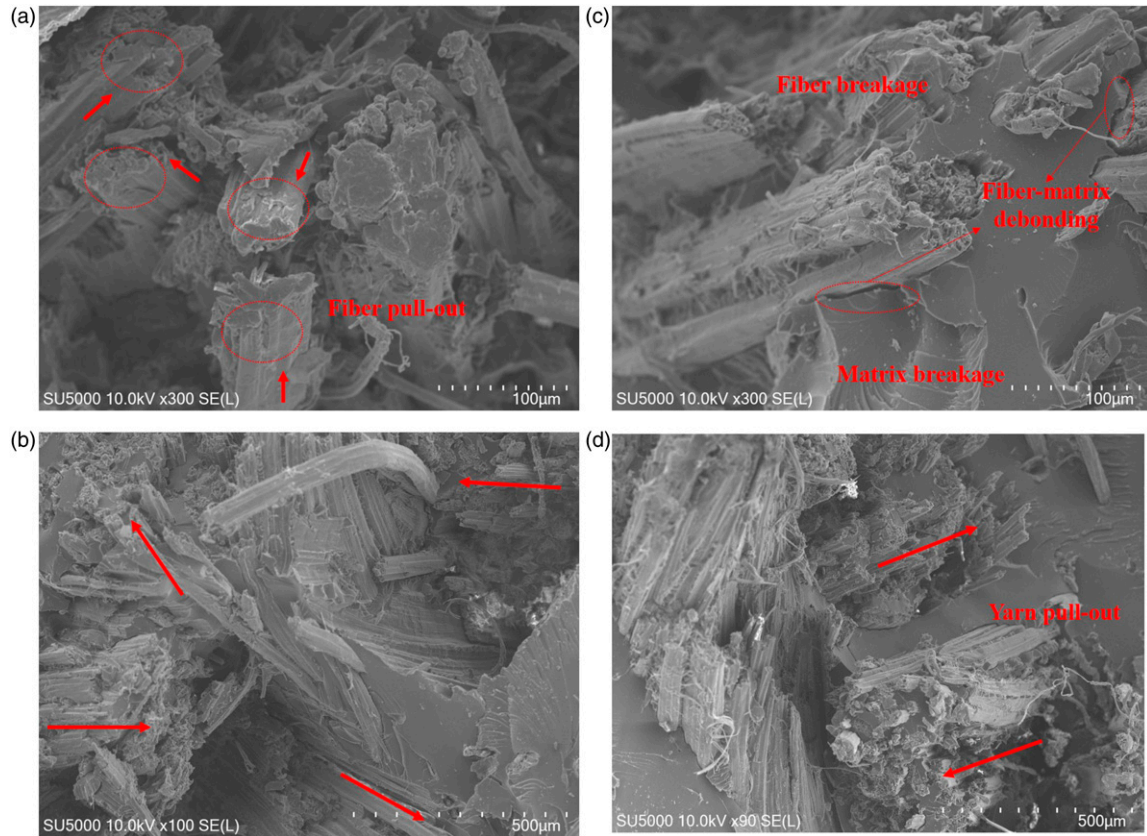


**Figure 17.** SEM micrographs of the 3D braided composite honeycomb after damage. (a) Typical yarn pull-out. (b) Closer view showing the fiber breakage, matrix breakage and fiber-matrix debonding. (c) Yarn bundles in four directions at the fracture surface. (d) Closer view showing the broken fiber in four different directions.

When the load is applied in *Y* direction, progressive damage occurs. In this instance, in addition to the load on the free walls, there is also the force on the joint walls. The load is transferred from the hypotenuse (free wall) to the vertical wall (joint wall) to the next hypotenuse. The joint wall length of Y-1 is longer, and it takes a longer distance to pass from one free wall to the next free wall, so the next node will be destroyed after one node is destroyed. For Y-2, the joint wall length is slightly reduced, but still progressive. For Y-3, the joint wall length is smaller and the shape of a cell is nearly like a diamond. The hypotenuse is basically in a line. The force transferred is instantaneous, so the failure occurs at the same time, and the sample collapses.

Therefore, it is concluded that 3D braided composite honeycomb exhibit shear-type failure. The main failure types include yarn pull-out, fibre pull-out, fiber breakage, matrix breakage, and fiber-matrix debonding. Increasing the joint wall length in the loading direction increases the progressive damage process. When the joint wall is small and the cell shape is close to a diamond or the joint wall is not parallel to the loading direction (the load is loaded in the *X* direction), a sudden brittle fracture occurs in the samples.

## Conclusions

In this study, self-made 3D braided jute/epoxy composite honeycombs were presented. The effects of different joint wall lengths on the in-plane compression properties were investigated. As the joint wall length increases, the size of the unit cell is bigger, and consequently the number of cells, in the honeycomb fabric manufactured according to the same number of braiding cycles, decreases. The following conclusions are drawn from the analysis:

1. The joint wall length has little effect on the mechanical properties. The more columns of the free wall, the greater the maximum load, and the more rows, the greater the displacement corresponding to the maximum load. At the same time, the smaller the angle between the free wall and the direction in which the load is applied, the higher the load-carrying performance. No matter the load applied along the *X*- direction or the *Y*- direction, the energy absorption performance increases with the decrease of the joint wall length and the increase of the number of cells.

2. All the samples exhibit shear-type failure modes. The main failure types include yarn pull-out, fibre pull-out, fiber breakage, matrix breakage, and fiber-matrix debonding. When the joint wall is parallel to the loading direction, cracks appear almost simultaneously. But when the joint wall is perpendicular to the loading direction, cracks appear sequentially. When the joint wall is too small and the shape of a cell is close to a diamond or the joint wall is not parallel to the loading direction (the load is loaded in the  $X$  direction), a sudden brittle fracture occurs in the samples.

To sum up, the best bearing capacity of 3D braided composite honeycombs in this study is demonstrated by the honeycomb with three columns of cells, called X-3. Its compressive maximum load is about 14.21 kN, and its total strain energy absorption is also the highest of about 44.97 J. The bearing capacity of the 3D braided composite honeycomb can be improved by increasing the number of cells and reducing the angle between the free wall and the loading direction to improve its load-bearing performance. The energy absorption performance of the structure can be strengthened by improving the toughness of the material, reducing the length of the joint wall, and increasing the number of unit cells. However, the joint wall cannot be too small or disappear.

### Declaration of conflicting interests

The author(s) declared no potential conflicts of interest with respect to the research, authorship, and/or publication of this article.

### Funding

The author(s) received no financial support for the research, authorship, and/or publication of this article.

### ORCID iDs

Li Qian-Qian  <https://orcid.org/0000-0001-9580-931X>  
 Yasmine Mosleh  <https://orcid.org/0000-0002-7322-1539>  
 Li Wei  <https://orcid.org/0000-0002-1561-166X>

### References

- Chandrasekaran NK and Arunachalam V. State of the art review on honeycomb sandwich composite structures with an emphasis on filler materials. *Polym Compos* 2021; 42(10): 5011–5020. DOI: [10.1002/pc.26252](https://doi.org/10.1002/pc.26252)
- Chen X, Yu G, Wang Z, et al. Enhancing out-of-plane compressive performance of carbon fiber composite honeycombs. *Compos. Struct* 2021; 255: 112984. DOI: [10.1016/j.compstruct.2020.112984](https://doi.org/10.1016/j.compstruct.2020.112984)
- Wei X, Xiong J, Wang J, et al. New advances in fiber-reinforced composite honeycomb materials. *Sci China Technol Sci* 2020; 63(8): 1348–1370. DOI: [10.1007/s11431-020-1650-9](https://doi.org/10.1007/s11431-020-1650-9)
- Vitale J P, Francucci G, Xiong J, et al. Failure mode maps of natural and synthetic fiber reinforced composite sandwich panels. *Compos. Part A Appl. Sci* 2017; 94: 217–225. DOI: [10.1016/j.compositesa.2016.12.021](https://doi.org/10.1016/j.compositesa.2016.12.021)
- Stocchi A, Colabella L, Cisilino A, et al. Manufacturing and testing of a sandwich panel honeycomb core reinforced with natural-fiber fabrics. *Mater. Des* 2014; 55: 394–403. DOI: [10.1016/j.matdes.2013.09.054](https://doi.org/10.1016/j.matdes.2013.09.054)
- Wei X, Li D and Xiong J. Fabrication and mechanical behaviors of an all-composite sandwich structure with a hexagon honeycomb core based on the tailor-folding approach. *Compos Sci Technol* 2019; 184: 107878. DOI: [10.1016/j.compscitech.2019.107878](https://doi.org/10.1016/j.compscitech.2019.107878)
- Pehlivan L and Baykasoğlu C. An experimental study on the compressive response of CFRP honeycombs with various cell configurations. *Compos. B. Eng* 2019; 162: 653–661. DOI: [10.1016/j.compositesb.2019.01.044](https://doi.org/10.1016/j.compositesb.2019.01.044)
- Wei X, Wu Q, Gao Y, et al. Composite honeycomb sandwich columns under in-plane compression: Optimal geometrical design and three-dimensional failure mechanism maps. *Eur J Mech A Solids* 2022; 91: 104415. DOI: [10.1016/j.euromechsol.2021.104415](https://doi.org/10.1016/j.euromechsol.2021.104415)
- Xiong J, Zhang M, Stocchi A, et al. Mechanical behaviors of carbon fiber composite sandwich columns with three dimensional honeycomb cores under in-plane compression. *Compos. B. Eng* 2014; 60: 350–358. DOI: [10.1016/j.compositesb.2013.12.049](https://doi.org/10.1016/j.compositesb.2013.12.049)
- Gu Q, Quan Z, Yu J, et al. Structural modeling and mechanical characterizing of three-dimensional four-step braided composites: A review. *Compos. Struct* 2019; 207: 119–128. DOI: [10.1016/j.compstruct.2018.09.065](https://doi.org/10.1016/j.compstruct.2018.09.065)
- Chen L, Tao X and Choy CL. RETRACTED: on the microstructure of three-dimensional braided preforms. *Compos Sci Technol* 1999; 59: 391–404. DOI: [10.1016/S0266-3538\(98\)00079-7](https://doi.org/10.1016/S0266-3538(98)00079-7)
- Goren A and Atas C. Manufacturing of polymer matrix composites using vacuum assisted resin infusion molding. *Arch. Mater. Sci. Eng* 2008; 34(2): 117–120.
- van Oosterom S, Allen T, Battley M, et al. An objective comparison of common vacuum assisted resin infusion processes. *Compos. Part A Appl. Sci* 2019; 125: 105528. DOI: [10.1016/j.compositesa.2019.105528](https://doi.org/10.1016/j.compositesa.2019.105528)
- Schilling PJ, Karedla BR, Tatiparthi A K, et al. X-ray computed microtomography of internal damage in fiber reinforced polymer matrix composites. *Compos Sci Technol* 2005; 65(14): 2071–2078. DOI: [10.1016/j.compscitech.2005.05.014](https://doi.org/10.1016/j.compscitech.2005.05.014)
- Zaini E S, Azaman M D, Jamali M S, et al. Synthesis and characterization of natural fiber reinforced polymer composites as core for honeycomb core structure: a review. *J. Sandw. Struct Mater* 2018; 22(3): 525–550. DOI: [10.1177/1099636218758589](https://doi.org/10.1177/1099636218758589)
- Wang H, Sun B and Gu B. Coupling effect of temperature and braided angle on compressive behaviors of 3D braided carbon-epoxy composite at low temperature. *J. Compos. Mater* 2016; 51(18): 2531–2547. DOI: [10.1177/0021998316674065](https://doi.org/10.1177/0021998316674065)
- Ingrole A, Hao A and Liang R. Design and modeling of auxetic and hybrid honeycomb structures for in-plane property enhancement. *Mater. Des* 2017; 117: 72–83. DOI: [10.1016/j.matdes.2016.12.067](https://doi.org/10.1016/j.matdes.2016.12.067)
- Wang AJ and McDowell DL. In-plane stiffness and yield strength of periodic metal honeycombs. *J Eng Mater Technol* 2004; 126(2): 137–156. DOI: [10.1115/1.1646165](https://doi.org/10.1115/1.1646165)

19. Jin T, Zhou Z, Liu Z, et al. Size effects on the in-plane mechanical behavior of hexagonal honeycombs. *Sci. Eng. Compos. Mater* 2016; 23(3): 301–307. DOI: [10.1515/secm-2014-0121](https://doi.org/10.1515/secm-2014-0121)
20. Tekoglu C, Gibson L J, Pardo T, et al. Size effects in foams: Experiments and modeling. *Prog. Mater Sci* 2011; 56(2): 109–138. DOI: [10.1016/j.pmatsci.2010.06.001](https://doi.org/10.1016/j.pmatsci.2010.06.001)
21. Li Q, Zhang H, Mosleh Y et al. Development and analysis of a three-dimensional braided honeycomb structure. *Text Res J* 2022; 004051752211395.
22. Atli B and Gandhi F. (2008). Energy absorption of cellular honeycombs with various cell angles under in-plane compressive loading. In: 49th AIAA/ASME/ASCE/AHS/ASC structures, structural dynamics, and Materials conference 16th AIAA/ASME/AHS adaptive structures conference 16t 7 - 10 April 2008, Schaumburg, IL.
23. Ashby MFMR and Medalist RFM. The mechanical properties of cellular solids. *Metall Trans A* 1983; 14(9): 1755–1769. DOI: [10.1007/BF02645546](https://doi.org/10.1007/BF02645546)
24. Ayanoglu MO, Tauhiduzzaman, Carlsson LA, et al. In-plane compression modulus and strength of Nomex honeycomb cores. *J. Sandw. Struct. Mater* 2021; 24(1): 627–642. DOI: [10.1177/10996362211021888](https://doi.org/10.1177/10996362211021888)
25. Dou H, Ye W, Zhang D, et al. Comparative study on in-plane compression properties of 3D printed continuous carbon fiber reinforced composite honeycomb and aluminum alloy honeycomb. *Thin-Walled Struct* 2022; 176: 109335. DOI: [10.1016/j.tws.2022.109335](https://doi.org/10.1016/j.tws.2022.109335)
26. Hu L, You F and Yu T. Effect of cell-wall angle on the in-plane crushing behaviour of hexagonal honeycombs. *Mater. Des* 2013; 46: 511–523. DOI: [10.1016/j.matdes.2012.10.050](https://doi.org/10.1016/j.matdes.2012.10.050)
27. Chen J, Fang H, Liu W, et al. Energy absorption of foam-filled multi-cell composite panels under quasi-static compression. *Compos. B. Eng* 2018; 153: 295–305. DOI: [10.1016/j.compositesb.2018.08.122](https://doi.org/10.1016/j.compositesb.2018.08.122)
28. Ha NS and Lu G. A review of recent research on bio-inspired structures and materials for energy absorption applications. *Compos. B. Eng* 2020; 181: 107496. DOI: [10.1016/j.compositesb.2019.107496](https://doi.org/10.1016/j.compositesb.2019.107496)
29. Atli-Veltin B and Gandhi F. Effect of cell geometry on the energy absorption of honeycombs under in-plane compression. *AIAA J* 2010; 48(2): 466–478. DOI: [10.2514/1.45021](https://doi.org/10.2514/1.45021)
30. Khan M K, Baig T and Mirza S. Experimental investigation of in-plane and out-of-plane crushing of aluminum honeycomb. *Mater. Sci. Eng: A* 2012; 539: 135–142. DOI: [10.1016/j.msea.2012.01.070](https://doi.org/10.1016/j.msea.2012.01.070)
31. Cricri G, Perrella M and Cali C. Honeycomb failure processes under in-plane loading. *Compos. B. Eng* 2013; 45(1): 1079–1090. DOI: [10.1016/j.compositesb.2012.07.032](https://doi.org/10.1016/j.compositesb.2012.07.032)
32. Ahmad S, Zhang J, Feng P, et al. Processing technologies for Nomex honeycomb composites (NHCs): a critical review. *Compos. Struct* 2020; 250: 112545. DOI: [10.1016/j.compstruct.2020.112545](https://doi.org/10.1016/j.compstruct.2020.112545)
33. Li S, Liu Z, Shim V P W, et al. In-plane compression of 3D-printed self-similar hierarchical honeycombs – static and dynamic analysis. *Thin-Walled Struct* 2020; 157: 106990. DOI: [10.1016/j.tws.2020.106990](https://doi.org/10.1016/j.tws.2020.106990)
34. Fang G, Chen C, Meng S, et al. Mechanical analysis of three-dimensional braided composites by using realistic voxel-based model with local mesh refinement. *J. Compos. Mater* 2018; 53(4): 475–487. DOI: [10.1177/0021998318786541](https://doi.org/10.1177/0021998318786541)